

Density structure of an active region and associated moss using Hinode/EIS

D. Tripathi¹, H. E. Mason¹, P. R. Young², G. Del Zanna³

¹ Department of Applied Maths and Theoretical Physics, University of Cambridge, Wilberforce Road, Cambridge CB3 0WA, UK
e-mail: [D.Tripathi; H.E.Mason]@damtp.cam.ac.uk

² STFC, Rutherford Appleton Laboratory, Chilton, Didcot, Oxfordshire OX11 0QX, UK
e-mail: P.R.Young@rl.ac.uk

³ Mullard Space Science Laboratory, University College London, Holmbury St. Mary, Dorking, Surrey RH5 6NT, UK
e-mail: gdz@mssl.ucl.ac.uk

Received 09 Nov 2007; accepted 03 Dec 2007

ABSTRACT

Context. Studying the problem of active region heating requires precise measurements of physical plasma parameters such as electron density, temperature etc. It is also important to understand the relationship of coronal structures with the magnetic field. The Extreme-ultraviolet Imaging Spectrometer (EIS) aboard Hinode provides a rare opportunity to derive electron density simultaneously at different temperatures.

Aims. We study the density structure and characterise plasma in active regions and associated moss regions. In addition we study its relationship to the photospheric magnetic field.

Methods. We used data recorded by the EIS, together with magnetic field measurements from the Michelson Doppler Imager (MDI) aboard SoHO and images recorded with the Transition Region And Coronal Explorer (TRACE) and X-Ray Telescope (XRT/Hinode).

Results. We find that the hot core of the active region is densest with values as high as $10^{10.5} \text{ cm}^{-3}$. The electron density estimated in specific regions in the active region moss decreases with increasing temperature. The moss areas were located primarily on one side of the active region, and they map the positive polarity regions almost exactly. The density within the moss region was highest at $\log T = 5.8 - 6.1$, with a value around $10^{10.0-10.5} \text{ cm}^{-3}$. The moss densities were highest in the strong positive magnetic field region. However, there was no such correlation for the negative polarity areas, where there was a large sunspot.

Key words. Sun: atmosphere, Sun: activity, Sun: corona, Sun: magnetic fields, Sun: transition region, Sun: UV radiation

1. Introduction

Active regions (ARs) are the brightest features seen on the Sun's surface when observing in ultra-violet and X-rays. Most of the high energy explosions, such as flares and coronal mass ejections (CMEs), originate from ARs (e.g., Tripathi et al. 2004; Tripathi 2006). Moreover, studying the physics of ARs can prove valuable for understanding the problem of coronal heating. There have been numerous models explaining coronal heating (see Klimchuk 2006, for a recent review); however, a solution remains elusive.

From the observational point of view, studying the problem of coronal heating requires precise and simultaneous measurements of the plasma parameters such as electron density, plasma flows and non-heating broadening etc at different temperatures. Various attempts have been made to investigate the above-mentioned parameters using previous instruments such as the Coronal Diagnostic Spectrometer (CDS; Harrison et al. 1995) aboard the Solar and Heliospheric Observatory (SoHO; Domingo et al. 1995). From diagnostic studies of eclipse observations and also early X-ray observations it was found that ARs have a hot and dense core (see e.g., Gabriel & Jordan 1975; Webb 1981). Mason et al. (1999) have produced a density map of an AR from CDS data using Si x $\lambda 356.0/\lambda 374.4$ density diagnostic (formed at $\log T = 6.1$) and found the highest densities in the AR core, with values over $2.3 \times 10^9 \text{ cm}^{-3}$. See other studies with CDS by Milligan et al. (2005) and Tripathi et al. (2006). It has also been found that the density and temperatures were higher in the regions of emerging and cancelling magnetic flux (Tripathi et al. 2006), similar to the conclusions derived from early X-ray observations (Webb & Zirin 1981). However, because of limited temperature coverage and a limited number of density and temperature-sensitive spectral lines, a comparison of electron densities at different temperatures was not possible.

A specific type of AR emission known as “moss” was clearly visible in 171 Å images (dominated by Fe ix and Fe x emission) taken by the Transition Region And Coronal Explorer (TRACE; Berger et al. 1999; de Pontieu et al. 1999). Morphological and dynamical aspects of this AR emission are described by Berger et al. (1999), who conclude that moss is emission from the upper transition region and moss regions are the foot points of hot coronal loops (see also Zhao et al. 2000) seen in X-ray emission. Later, using the spectroscopic data for an AR from the CDS, Fletcher & de Pontieu (1999) show that the moss region has a temperature range of $0.6 - 1.5 \times 10^6 \text{ K}$ and is associated with the footpoints of hot loops. They also show that the electron density is $2.5 \times 10^9 \text{ cm}^{-3}$ at a temperature of about $1.3 \times 10^6 \text{ K}$.

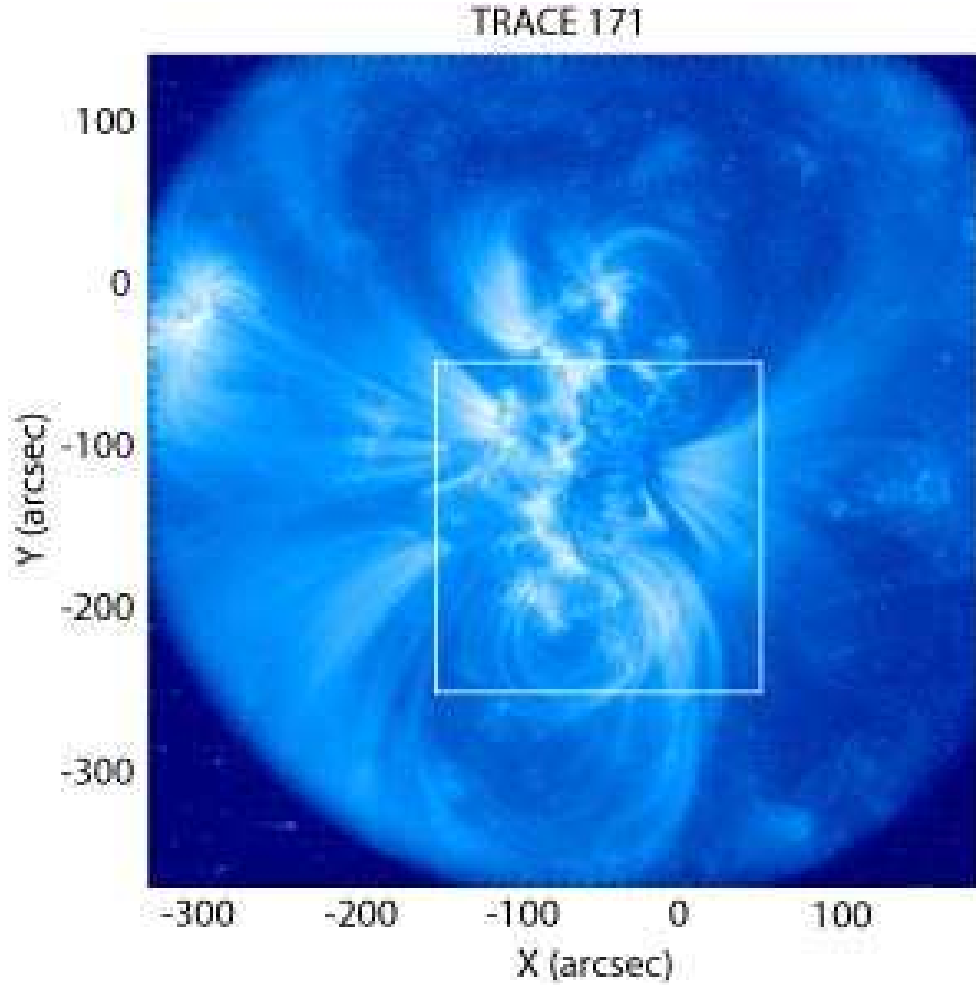


Fig. 1. TRACE at 171 Å showing the AR studied here, 2007 May 01. The overplotted box shows the region that was rastered by EIS.

In order to characterise the plasma emission from the moss region more precisely, it is important to simultaneously determine the densities over a range of temperatures. The Extreme-ultraviolet Imaging Telescope (EIS; Culhane et al. 2007) aboard Hinode, having very good spatial and spectral resolution with a broad temperature coverage, provides an excellent opportunity to study the physical plasma parameters in ARs, in particular in these moss regions. Using EIS data, Warren et al. (2007) find that the density in the moss regions can be as high at 10^{11} cm^{-3} at a temperature of $\log T = 6.1$ MK. They did not, however, discuss the association of the moss with the magnetic field or densities derived over a wide temperature range. In this paper we study the density structure of an on-disk AR and associated moss regions observed on May 1, 2007 using Hinode/EIS. We determine the density variation as a function of temperature and also study the relationship between density structure and photospheric magnetic field structures using data recorded from the Michelson Doppler Imager (MDI; Scherrer et al. 1995) aboard SoHO.

2. Observations and data preparation

The EIS aboard Hinode provides spectroscopic and imaging observations of the solar corona and transition region in two wavelength channels. The first detector covers the wavelength range 246–292 Å (CCD-A) and the second covers 170–211 Å (CCD-B), providing observation in a broad range of temperature ($\log T = 5.8 - 6.7$ MK). The EIS provides high cadence images of the transition region and the corona using 40'' and 266'' slots. Monochromatic images can be obtained by rastering with a slit (1'' or 2''). For other technical details, see Culhane et al. (2007).

In this paper we have used the EIS study we designed, “cam_artb_cds_a”, which comprises 22 spectral windows covering spectral lines over a broad range of temperatures. This study uses the 2'' slit with an exposure time of 10 seconds and was run on an on-disk AR for several days in May 2007. Here we study the observations made on May 1, 2007. The raster covered a field of view (FOV) of $200'' \times 200''$ in 20 minutes. Figure 1 shows the AR as imaged by the TRACE 171 Å filter. Most of the bright, mottled emission in the core of the AR (running approximately north/south) comes from areas of “moss”. The box in the TRACE image shows the region which was rastered by EIS using the 2'' slit. The EIS raster mainly covers the central part of the AR.

The study “cam_artb_cds_a” includes many different density sensitive lines over a range of temperatures. We applied standard processing routines, namely “eis_prep.pro” and have fitted the spectrum for each pixel using the routine “eis_auto_fit.pro”, both of which are available in the solar software tree. The line list published in Tripathi et al. (2007) was used to derive the electron density.

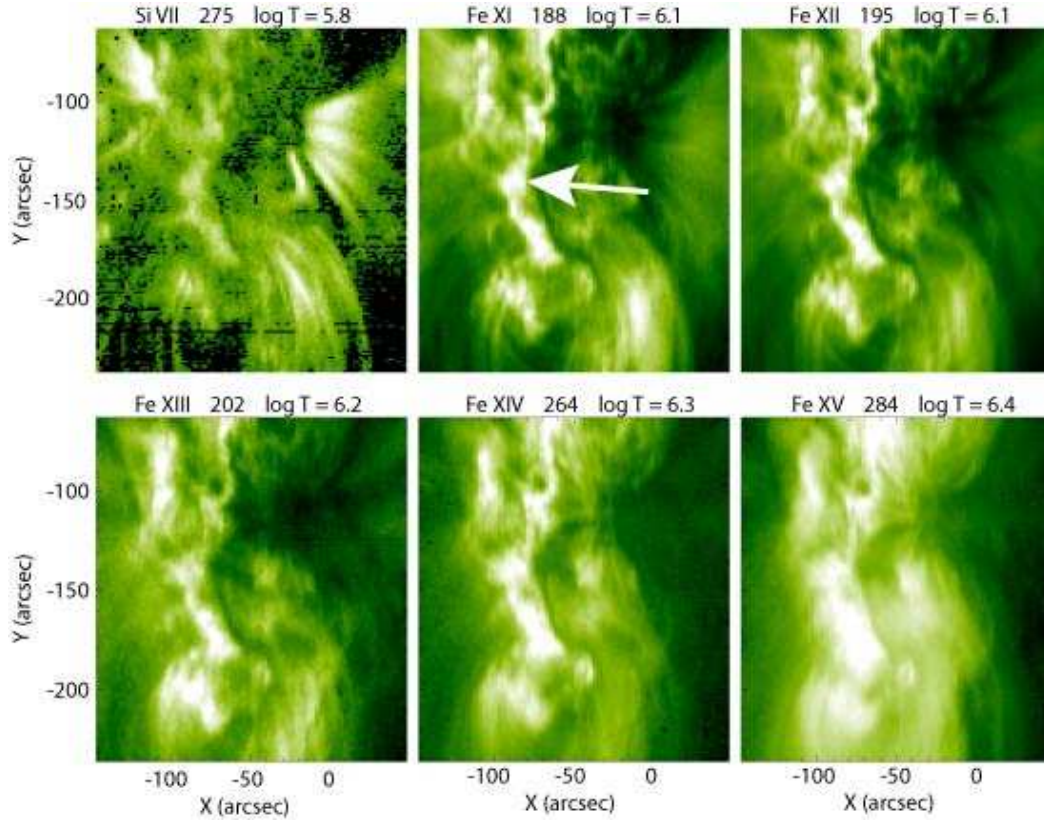


Fig. 2. Monochromatic images recorded by the EIS. The title of each panel displays the ion name and the respective wavelengths in which these images were created and their peak temperature formation. The arrow in the top middle image indicates a moss region.

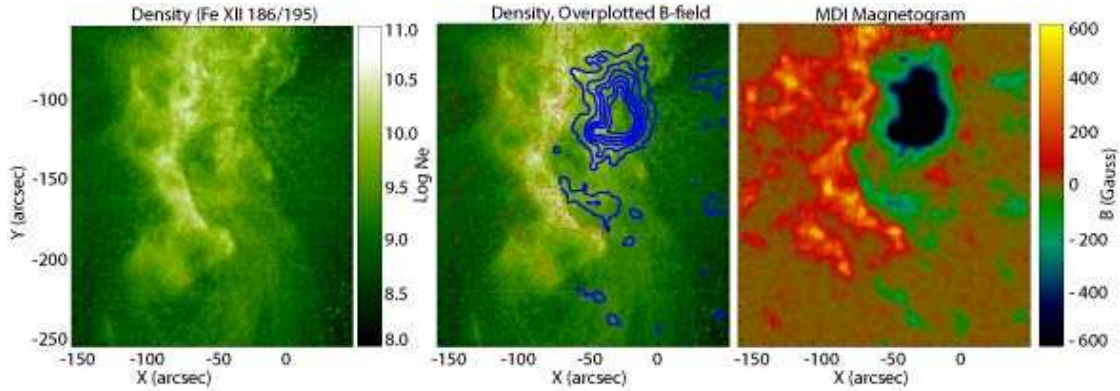


Fig. 3. Left panel: Electron density map (cm^{-3}) derived using the line ratios Fe XII 186 and 195 Å. Middle Panel: Electron density map overplotted with magnetic field contours. Red contours correspond to positive polarity region whereas blue contours represent negative polarity regions. Right Panel: MDI magnetogram of the corresponding region.

The electron density values were obtained using the theoretical line intensity ratios calculated using CHIANTI (Dere et al. 1997; Landi et al. 2006).

Some of the spectral lines used in this study are blended with other lines so care must be taken when deriving the plasma parameters. The Mg VII $\lambda 278$ line is blended with a Si VII line, the Fe XIII $\lambda 203$ is blended with another Fe XII line and Fe XIV $\lambda 274$ line is blended with a Si VII line. These blends were taken into account when fitting the lines. The Fe XII blend from Fe XIII $\lambda 203$ was removed by fitting a double Gaussian. However, we have used another Si VII $\lambda 275$, which is quite a strong line, to remove blends from the Mg VII $\lambda 278$ and Fe XIV $\lambda 274$ lines. The Fe XII $\lambda 186$ and $\lambda 195$ lines are self blends and care has to be taken when deriving the densities using Fe XII $\lambda 186$ and $\lambda 195$ lines, because this can have a substantial influence on high density regions. For more details on the removal of blends from these spectral lines, see Young et al. (2007). The Fe XII line intensities were problematic for many years, but new work by Del Zanna & Mason (2005) has resolved these discrepancies. There is an error in one of the Fe XIII atomic data files in CHIANTI v.5.2 that leads to the Fe XIII 203/202 ratios yielding incorrect densities. The corrected file was used for the present analysis and will be made available in the next CHIANTI release.

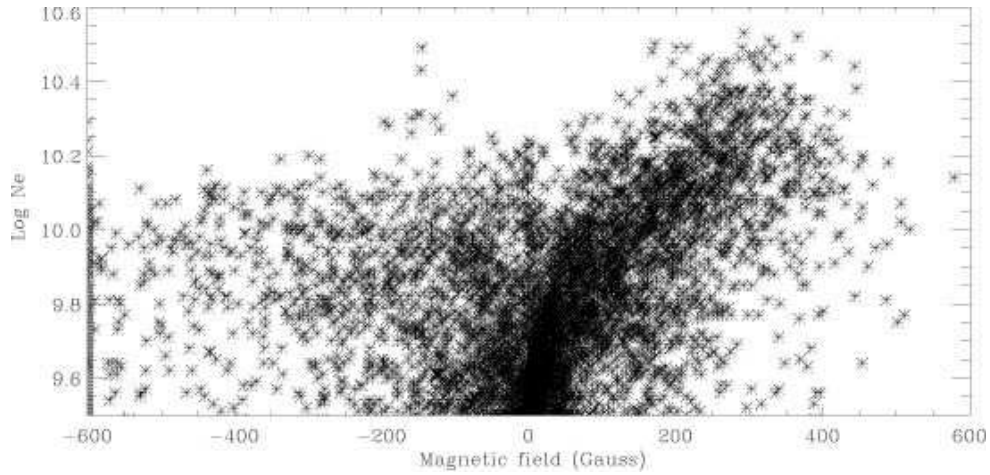


Fig. 4. Plot showing the variation of electron density (cm^{-3}) and magnetic field strength.

For comparing the intensity and density structures with photospheric magnetic field, we have used magnetograms recorded by the MDI. For this comparison a co-alignment of the data taken from different spacecrafts is necessary, which is not straightforward to achieve. In this analysis for co-aligning purposes, we used the full-disk image closest in time of observations recorded by the Extreme-ultraviolet Imaging Telescope (EIT; Delaboudinière et al. 1995) as a reference. The EIT 195 Å image was co-aligned with an image of the Fe XII $\lambda 195$ line intensities from EIS. There is a spatial difference between the images obtained with the two wavelength bands of EIS (CCD1 and CCD2). The image in the Fe XII $\lambda 195$ line emission (CCD1) was co-aligned with that recorded in Si X $\lambda 261$ line emission (CCD2). This co-alignment was then used for all images from CCD2. Since images obtained by MDI are full disk, the pointing information is reliable.

3. Results and discussion

Figure 2 displays monochromatic images recorded simultaneously using the EIS 2'' slit. The image recorded in the Si VII $\lambda 275$ line (top left image) shows the structure of the AR at the transition region temperature ($\log T = 5.8$). The very core of the AR as well as the plume-like structures (on the right-hand side of the image), which emanate from a sunspot region, can be clearly seen. The Si VII $\lambda 275$ line image is very similar to the corresponding TRACE 171 Å pass-band image shown in Fig. 5. As we go higher in the temperature such as Fe XI ($\log T = 6.1$), Fe XII ($\log T = 6.1$), Fe XIII ($\log T = 6.2$), Fe XIV ($\log T = 6.3$), and Fe XV ($\log T = 6.4$), AR structures become more complex. This confirms the conclusions from early observations (e.g., Gabriel & Jordan 1975; Webb 1981; Mason et al. 1999; Milligan et al. 2005; Tripathi et al. 2006) that the core of an AR is very hot.

The moss emission is seen running north/south in the left-hand side of the TRACE image (Fig. 5) and also in Fig. 2. It seems that the AR moss is seen clearly only on one side of the AR. With the EIS (Fig. 2), the moss emission can be seen at many different temperatures, $\log T = 5.8$ – 6.3 MK.

The left panel of Fig. 3 displays the density map of the AR derived using the line ratios (Fe XII, 186.8/195.1). The Fe XII line ratios are sensitive to the density range from 10^7 to 10^{12} cm^{-3} , which provides an opportunity to measure densities in the core, as well as in the outer regions of ARs. As is evident from the density map, the density is highest in the core of the AR and reaches values up to $10^{10.5} \text{ cm}^{-3}$. We also derived the density maps using line ratios from Mg VII ($\lambda 280/\lambda 278$), Fe XIII ($\lambda 203/\lambda 202$), and Fe XIV ($\lambda 264/\lambda 274$) and found that the densities in the core of the ARs were highest at all these temperatures (Tripathi et al. 2007).

The density maps obtained using line ratios were compared with the photospheric magnetic field configuration. The middle panel of Fig. 3 displays magnetic field contours overplotted on density maps and the right panel displays magnetic field map of the region. The red contours overplotted on the density map represent the positive polarity and blue contours represent the negative polarities. While displaying the magnetic field map of the region, the magnetic field strength is scaled between ± 600 G. We note that in the positive polarity region, the density maps almost correlate with the magnetic field strength exactly. Figure 4 shows a scatter plot of electron density vs magnetic field strength showing a strong correlation between electron density and positive magnetic field strength. There is no similar correlation between electron density and magnetic field strength for negative polarities. An interesting point is that the densities are high only towards the positive polarity side where most of the moss emission is located. On the negative polarity side, it is possible that the presence of a large sunspot could have an influence on this phenomenon.

Figure 5 displays a TRACE 171 Å image showing the specific regions inside and outside moss for which we have carried out a further study of the electron densities using line ratios at different temperatures. Figure 6 displays average densities calculated in the marked regions plotted against temperature. Regions A, B, D, and E are in bright moss regions on the positive polarity side of the AR. Inside the moss regions, we find that the average density is about 10^{10} cm^{-3} for $\log T = 5.8$ – 6.1 , and it drops to around $10^{9.5} \text{ cm}^{-3}$ at $\log T = 6.3$. Regions C, H, and G are in fainter moss regions, which have somewhat lower electron density values of around $10^{9.5} \text{ cm}^{-3}$ at $\log T = 5.8$ – 6.1 . Regions F and I are outside the moss regions. Coronal loops are evident in region I. As can be seen from the plots, the electron densities are higher in all regions (inside and outside moss) at lower temperatures and decrease with temperature. For region F, we did not have enough counts for Mg VII lines and therefore could not derive the densities

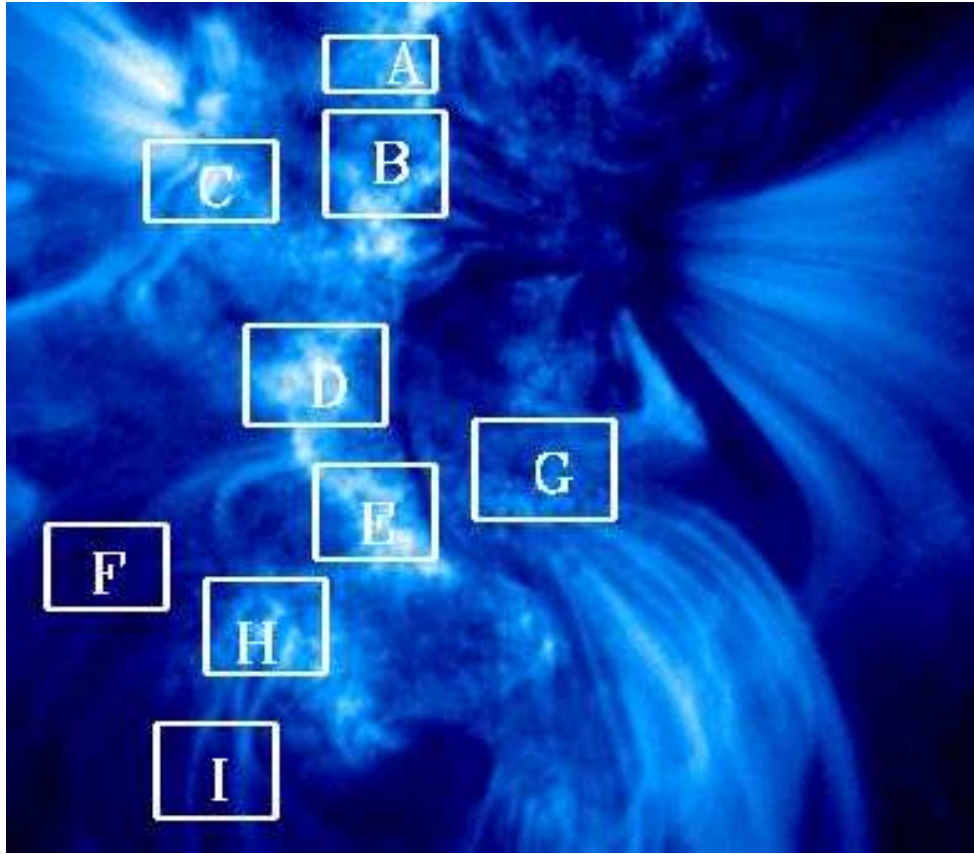


Fig. 5. TRACE at 171 Å passband showing the regions in which the average electron densities were investigated further using different line ratios.

at that temperature. However, the electron density derived in region F using Fe XII, Fe XIII and Fe XIV is just below $10^{9.0} \text{ cm}^{-3}$, close to the one for region I at the same temperatures ($\log T = 6.1\text{--}6.3$).

4. Conclusions

The EIS provides an excellent opportunity to study the physical plasma parameters simultaneously at many different temperatures from the transition region to the corona. In this paper we have studied the density structure in an AR and associated moss observed on May 1, 2007. We compared the derived densities with the magnetic field structures observed at the photosphere. We found that the densities are highest in the core of the ARs across a range of temperatures.

This observations show that the associated moss is located only towards one side (positive polarity) of the AR. Using spectral line ratios, we find that the density inside the moss region is highest ($10^{10.0\text{--}10.5} \text{ cm}^{-3}$) at $\log T = 5.8\text{--}6.1$. The electron density decreases to $10^{9.5} \text{ cm}^{-3}$ at higher temperatures. In non-moss regions, where coronal loops are evident, the electron density is around $10^{9.0} \text{ cm}^{-3}$ at $\log T = 6.1\text{--}6.3$. Following a careful co-alignment, a comparison with the MDI magnetogram reveals that the high density is correlated with the strong positive field regions where moss is located. However the negative field region, which includes a large sunspot, shows no such correlation.

Acknowledgements. We would like to thank the referee for constructive comments. DT, HEM, and GDZ acknowledge the STFC. Hinode is a Japanese mission developed and launched by ISAS/JAXA, collaborating with NAOJ as a domestic partner and NASA and STFC (UK) as international partners. Scientific operation of the Hinode mission is conducted by the Hinode science team organised at ISAS/JAXA. This team mainly consists of scientists from institutes in the partner countries. Support for the post-launch operation is provided by JAXA and NAOJ (Japan), STFC (U.K.), NASA, ESA, and NSC (Norway)

References

- Berger, T. E., de Pontieu, B., Fletcher, L., et al. 1999, *Sol. Phys.*, 190, 409
- Culhane, J. L., Harra, L. K., James, A. M., et al. 2007, *Sol. Phys.*, 243, 19
- de Pontieu, B., Berger, T. E., Schrijver, C. J., & Title, A. M. 1999, *Sol. Phys.*, 190, 419
- Del Zanna, G. & Mason, H. E. 2005, *A&A*, 433, 731
- Delaboudinière, J.-P., Artzner, G. E., Brunaud, J., et al. 1995, *Sol. Phys.*, 162, 291
- Dere, K. P., Landi, E., Mason, H. E., Monsignori Fossi, B. C., & Young, P. R. 1997, *A&AS*, 125, 149
- Domingo, V., Fleck, B., & Poland, A. I. 1995, *Sol. Phys.*, 162, 1
- Fletcher, L. & de Pontieu, B. 1999, *ApJ*, 520, L135
- Gabriel, A. H. & Jordan, C. 1975, *MNRAS*, 173, 397
- Harrison, R. A., Sawyer, E. C., & Carter, M. K. e. a. 1995, *Sol. Phys.*, 162, 233

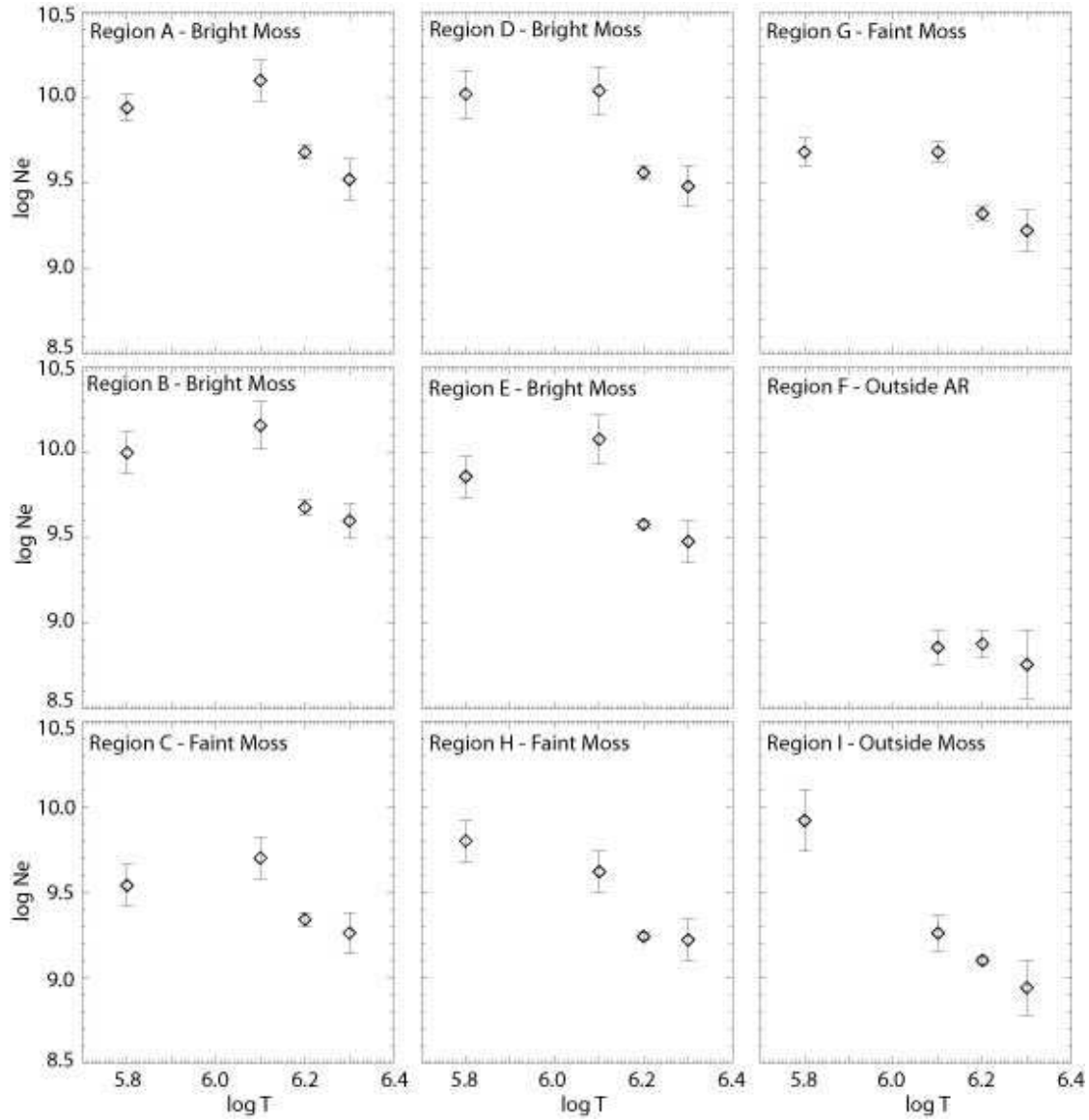


Fig. 6. Estimated electron densities (cm^{-3}) at different temperatures for the regions marked in Fig. 5. Error bars are estimated by assuming an error of 10% in the line intensities.

- Klimchuk, J. A. 2006, *Sol. Phys.*, 234, 41
 Landi, E., Del Zanna, G., Young, P. R., et al. 2006, *ApJS*, 162, 261
 Mason, H. E., Landi, E., Pike, C. D., & Young, P. R. 1999, *Sol. Phys.*, 189, 129
 Milligan, R. O., Gallagher, P. T., Mathioudakis, M., Keenan, F. P., & Bloomfield, D. S. 2005, *MNRAS*, 363, 259
 Scherrer, P. H., Bogart, R. S., Bush, R. I., et al. 1995, *Sol. Phys.*, 162, 129
 Tripathi, D. 2006, *Journal of Astrophysics and Astronomy*, 27, 193
 Tripathi, D., Bothmer, V., & Cremades, H. 2004, *A&A*, 422, 337
 Tripathi, D., Mason, H. E., & Young, P. R. 2006, in *ESA Special Publication*, Vol. 617, SOHO-17. 10 Years of SOHO and Beyond
 Tripathi, D., Mason, H. E., Young, P. R., Chifor, C., & Del Zanna, G. 2007, in *Announcing First Results from Hinode*, ASP Conference Series Ed. Sarah Mathews et al. in press
 Warren, H. P., Winebarger, A. R., Mariska, J. T., Doschek, G. A., & Hara, H. 2007, *ArXiv e-prints*, 0709
 Webb, D. F. 1981, Chap 7 *Solar Active Regions*, Colorado Associated University Press, Colorado, Ed. F.Q. Orrall
 Webb, D. F. & Zirin, H. 1981, *Sol. Phys.*, 69, 99
 Young, P. R., Del Zanna, G., Mason, H. E., et al. 2007, *ArXiv e-prints*, 0706
 Zhao, X. P., Hoeksema, J. T., Kosovichev, A. G., Bush, R., & Scherrer, P. H. 2000, *Sol. Phys.*, 193, 219